

Pretrained Battery Transformer (PBT): A battery life prediction foundation model

Ruifeng Tan^{1,2}, Weixiang Hong¹, Jia Li^{3*}, Jiaqiang Huang^{1,4,5*} and Tong-Yi Zhang^{6*}

¹Guangzhou Municipal Key Laboratory of Materials Informatics and Sustainable Energy and Environment Thrust, The Hong Kong University of Science and Technology (Guangzhou), Nansha, Guangzhou, 511400, Guangdong, P.R. China.

²Department of Computer Science & Engineering, The Hong Kong University of Science and Technology, Clear Water Bay, Kowloon, 999077, Hong Kong, P.R. China.

³Guangzhou Municipal Key Laboratory of Materials Informatics and Data Science and Analytics Thrust, The Hong Kong University of Science and Technology (Guangzhou), Nansha, Guangzhou, 511400, Guangdong, P.R. China.

⁴Academy of Interdisciplinary Studies, The Hong Kong University of Science and Technology, Clear Water Bay, Kowloon, 999077, Hong Kong, P.R. China.

⁵Guangzhou HKUST Fok Ying Tung Research Institute, Nansha District, Guangzhou, 511458, Guangdong, P.R. China.

⁶Material Genome Institute, Shanghai University, 333 Nanchen Road, Shanghai 200444, P.R. China; Guangzhou Municipal Key Laboratory of Materials Informatics, Advanced Materials Thrust, and Sustainable Energy and Environment Thrust, The Hong Kong University of Science and Technology (Guangzhou), Nansha, Guangzhou, 511400, Guangdong, P.R. China.

*Corresponding authors.

E-mails: jjalee@ust.hk; seejhuang@hkust-gz.edu.cn; mezhangt@hkust-gz.edu.cn

Abstract

Early prediction of battery cycle life is essential for accelerating battery research, manufacturing, and deployment. Although machine learning methods have shown encouraging results, progress is hindered by data scarcity and heterogeneity arising from diverse aging conditions. In other fields, foundation models (FMs) trained on diverse datasets have achieved broad generalization through transfer learning, but no FMs have been reported for battery cycle life prediction yet. Here we present the Pretrained Battery Transformer (PBT), the first FM for battery life prediction, developed through domain-knowledge-encoded mixture-of-expert layers. Validated on the largest public battery life database, PBT learns transferable representations from 13 lithium-ion battery (LIB) datasets, outperforming existing models by an average of 19.8%. With transfer learning, PBT achieves state-of-the-art performance across 15 diverse datasets encompassing various operating conditions, formation protocols, and chemistries. This work establishes a foundation model pathway for battery lifetime prediction, paving the way toward universal battery lifetime prediction systems.

Introduction

Rechargeable batteries are central to the low-carbon energy transition, underpinning electric vehicles, grid storage and portable electronics¹⁻⁵. In 2020, shipments of LIBs for electric vehicles alone exceeded 140 GWh, and the total shipments are projected to reach 4700 GWh by 2030^{6,7}. Alongside LIBs, alternative chemistries such as sodium-ion, zinc-ion and full-solid-state batteries are gaining attention for their potential advantages in cost and safety⁸⁻¹⁰. Nevertheless, all rechargeable batteries inevitably degrade due to intrinsic electrochemical processes¹¹⁻¹³, leading to capacity fade and stability loss that raise user anxiety and safety concerns^{12,14,15}. Thus, aged batteries retire from high-demand applications like electric vehicles when they reach the end of life¹⁶⁻¹⁸. The battery lifetime is typically measured by the critical number of charge-discharge cycles, at which the battery capacity falls to 80% of the nominal capacity^{11,15}. Conventional battery degradation tests are time-consuming, often taking months to years, which impede the innovative design and

development of batteries¹². Accurate early battery cycle life prediction is therefore essential for battery optimization, production and utilization^{5,14,15,19}.

Data-driven methods have shown impressive results for early prediction of battery cycle life^{11,12,15,20-27}. Early efforts relied on handcrafted features derived from voltage-current profiles^{15,22,25,27,28} or additional characterizations^{24,29}, combined with classic machine learning. While effective in some datasets, these methods require substantial expert efforts tailored to individual datasets and often fail on datasets with different battery specifications and usage profiles^{11,20,21,23}. Neural networks overcome this limitation by learning directly from raw voltage-current profiles and, in general, outperform feature-engineered models^{11,12,20,21,30,31}. For example, CyclePatch¹² explicitly captures recurring cycle patterns in degradation tests, and achieves the leading performance across 18 neural network models. Despite these progresses, data-driven lifetime prediction models tend to fail due to two challenges: one is the intrinsic data scarcity of battery life data and the other is the data heterogeneity arising from diverse aging factors, including cathode materials, anode materials, electrolytes, manufacturing processes, formation protocols, and operating conditions^{11,12}. Especially, the data heterogeneity often induces data distribution differences between training and testing data, a phenomenon known in machine learning as domain shift, which often undermines model performance^{5,32}. Practical cycle life prediction models must therefore consider both data scarcity and heterogeneity.

Existing works handle data scarcity and heterogeneity through transfer learning, if different datasets share latent knowledge that can be transferred from source domains to target domains. The transfer learning methods can be categorized into fine-tuning^{20,33} and domain adaptation^{11,34}. Fine-tuning first pretrains a model on source domains and then fully or partially updates model parameters on target domains. For instance, Ma et al.²⁰ pretrained a neural network composed of convolutional neural network (CNN) and long short-term memory on one dataset and fine-tuned it on 22 target cells subjected to different discharge protocols. More advanced approaches fall under domain

adaptation, which simultaneously leverages source-domain and target-domain data to mitigate domain shift by encouraging transferable feature representations during model training. For instance, Zhang et al.³⁴ used domain-adversarial training to promote domain-invariant embeddings by constructing a domain classifier with gradient reversal mechanisms to alleviate domain-specific information. A recent study¹¹ proposed BatLiNet, which assumes that pairwise differences in feature representations correlate with pairwise differences in lifetimes and hence embeds pairwise differences of LiFePO₄ (LFP)/graphite cells with target cells into feature representations. Despite the encouraging results achieved by transfer learning, current models lack capability to integrate information across diverse datasets, which ultimately constrains transfer performance due to the lack of extensive source-domain knowledge.

In natural language processing³⁵⁻⁴¹ (NLP) and computer vision⁴²⁻⁴⁵ (CV) fields, foundation models (FMs) have emerged as models equipped with a wide range of general knowledge and patterns that serve as the foundation for a wide range of downstream applications^{46,47}. With transfer learning, these models exhibit broad utility and constitute indispensable components in many state-of-the-art NLP and CV systems⁴⁸⁻⁵². Nevertheless, the success of FMs hinges on architectures tailored to domain-specific data: DeepSeek^{35,41} and GPTs^{39,40} employ transformers variants optimized for text, whereas CV foundation models^{42,44,45,53} use convolutional neural networks or vision transformers. Moreover, although aggregating nearly all public battery life datasets yields coverage across diverse aging scenarios (various formation protocols^{25,54}, depth of discharge⁵⁵⁻⁵⁸, charge protocols^{14,15,55,57-62}, discharge protocols^{20,55,57,61-64}, stress factors⁵⁶, materials^{61,63,64}, operation temperatures^{56,58}, chemistries of LIBs and beyond¹²), the data volume remains 990 cells, far smaller compared to the datasets used in NLP and CV. Developing cycle life prediction FM is therefore both challenging and essential, with potential powerful applications in the ion battery development and downstream industries.

In this study, we present the first, to our knowledge, widely transferable foundation model for battery cycle life prediction: the

Pretrained Battery Transformer (PBT). Underpinning PBT is BatteryMoE, which is a mixture-of-expert layer tailored for capturing universal representation for battery life data from a collection of diverse battery life datasets. PBT is pretrained on 13 LIB datasets and achieves superior performance across leave-out test sets in comparison with previous leading models, demonstrating its mastery of the most comprehensive battery life knowledge. Transferability tests across the LIB datasets show that PBT has state-of-the-art performance power in a wide range of application scenarios, including 165 aging conditions represented by various LIB chemistries, charge protocols, discharge protocols, formation protocols, stress factors, and operation temperatures. Furthermore, PBT is applied to the 3 datasets of zinc-ion batteries, sodium-ion batteries and industrial large-capacity LIBs, outside from the pretraining data and it still delivers consistent superiority, underscoring its generalizability.

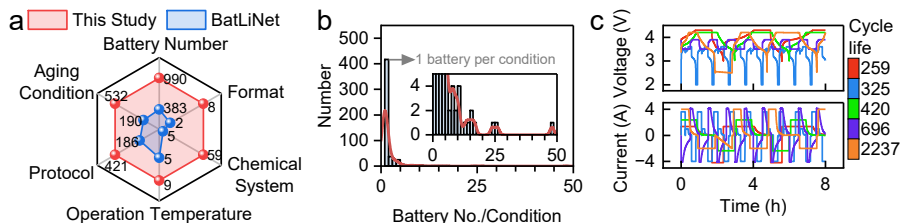


Fig. 1 | Data covered in this study and challenges arising from data scarcity and heterogeneity. **a**, Comparison of data statistics between this study and the second largest-scale battery cycle life prediction study (BatLiNet¹¹). It should be noted that some batteries collected by BatLiNet were not degraded to 80% of nominal capacity and are thus removed from the statistics¹². **b**, Distribution of battery aging condition density to illustrate the aging condition sharing, showing the peak over 400 at one battery per condition. In this work, we consider battery format, anode, cathode, electrolyte, formation protocols, charge protocols, discharge protocols, operation temperature, and manufacturer as aging factors, and a different in any aging factor produces a different aging condition. **c**, Cycling patterns of five batteries under five distinct aging conditions (see Supplementary Note 1) during the first eight hours, implying the diversity of cycling data patterns arising from hundreds of aging conditions.

Datasets and task definition

To demonstrate the capability of PBT in learning universal representation for battery life data, we compiled the largest and mostly diverse battery life database consisting of 16 publicly available datasets^{12,14,15,20,25,54,56-58,60,61,63,65-67}, including various formation protocols^{25,54}, depth of discharge⁵⁵⁻⁵⁸, charge protocols^{14,15,55,57-62}, discharge protocols^{20,55,57,61-64}, stress factors⁵⁶, materials^{61,63,64}, operation temperatures^{56,58}, chemistries of LIBs and beyond¹². As shown in Fig. 1a, in comparison with the previous largest database¹¹, our database contains 2.58 times batteries, 2.8 times aging conditions, 2.26 times charge–discharge protocols, 1.8 times operating temperatures, 11.8 times chemical systems, and 4 times physical formats (see Data availability for data preprocessing).

Despite this unprecedented size scale, our database still faces the challenge of data scarcity and heterogeneity: it contains only 990 batteries spanning 532 distinct aging conditions, of which 417 are represented by single cells (Fig. 1b), and thereby is a rigorous testbed

for evaluating PBT’s ability to learn robustly under data scarcity and heterogeneity.

Our goal is to develop a unified foundation model for early cycle life prediction for a wide spectrum of early prediction settings discussed in the literature^{11,21,24,31}. Given the first N charge–discharge cycles, with N being any integer ≤ 100 , the model predicts the cycle life—defined as the number of cycles at which the discharge capacity falls to 80% of nominal capacity.

Overview of pretrained battery transformer (PBT)

As illustrated in Fig. 1a and Fig. 1b, the database comprises hundreds of distinct aging conditions, most of which are represented by data from a single cell. These aging conditions induce diverse cycling patterns that can result in either convergent or highly divergent cell lifetimes (Fig. 1c), underscoring the necessity of capturing a broad spectrum of pattern–lifetime relationships. Clearly, learning such heterogeneous data is inherently challenging.

To address these challenges, we develop the Pretrained Battery Transformer (PBT) with BatteryMoE as its core module—a neural component that embeds battery knowledge to guide learning across heterogeneous battery life data. BatteryMoE decomposes complex pattern–lifetime relationships into interpretable aspects inspired by established battery knowledges^{15,20,23,55,58,68}, grouping batteries accordingly and enabling the training of a set of neural networks specialized in different groups. Outputs from relevant neural networks are then aggregated to model the cycling behavior of each battery. This approach facilitates efficient learning across heterogeneous mappings while preserving condition-specific knowledge, thereby improving both generalization and transferability.

As illustrated in Fig. 2a, BatteryMoE comprises two main components: a battery-knowledge-encoded gate network (Battery gate) and a set of battery-knowledge-informed expert networks. The architecture is inspired by the mixture-of-experts (MoE) paradigm that underpins large language models⁶⁹ but extends it through explicit integration of battery-knowledge priors. Conventional MoE

architectures rely solely on data-driven learning to assign input embeddings to experts, which could be ineffective for battery life prediction given the limited data volume and complex voltage–current dynamics (Supplementary Fig. 1). In contrast, BatteryMoE encodes battery knowledge through two complementary encoders (efficacy of both encoders are validated via ablation studies in Supplementary Fig. 1): (i) Soft encoder guides the gate network via knowledge-based pattern decomposition that produces informative representations of cycling behaviors, and (ii) Hard encoder imposes physically meaningful routing constraints by filtering irrelevant experts through knowledge-based weight selection. Together, these encodings enable BatteryMoE to learn transferable representations under scarce and heterogeneous aging data, forming the core of the Pretrained Battery Transformer.

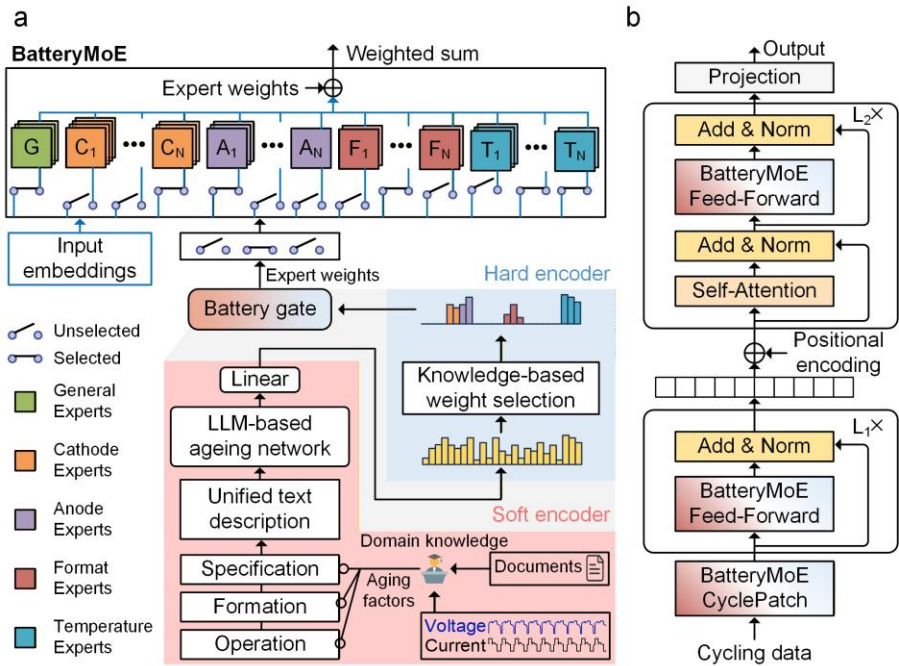


Fig. 2 | Overview of BatteryMoE and PBT. a, BatteryMoE includes a set of experts and the battery gate, which receives the representations from the hard encoder and soft encoder and delivers input embeddings to selected experts. **b**, The data flow and overview of architecture of PBT.

Soft encoder (pink region in Fig. 2a) generates informative embeddings that replace direct voltage–current inputs to the gate network. Ten aging factors, dominating the cycling data patterns, are identified in the present work and grouped into three categories: Specifications (cathode, anode, electrolyte, nominal capacity, format, manufacturer), Formation (formation protocol), and Operation (charge protocol, discharge protocol, and temperature). Rather than rigidly embedding these as categorical or continuous variables, BatteryMoE employs a unified text-based template (Supplementary Fig. 2) that flexibly describes each aging condition. The completed templates are processed by an LLM-based aging embedder, which converts textual descriptions into vector representations. These vectors exhibit meaningful clustering across batteries (Supplementary Fig. 3), reflecting the LLM’s prior knowledge of battery aging factors and facilitating downstream learning of their interactions. The resulting vector representations are then used by a linear layer to produce initial expert weights. Additional aging factors such as stacking stress⁷⁰ and coating processes⁷¹ can be incorporated similarly, though they are not considered in this work due to their absence in the collected datasets.

Hard encoder encodes battery knowledge via hard-coding routing rules on four key aging factors—cathode, anode, physical format, and operating temperature. For categorical factors (cathode, anode, and format), BatteryMoE constructs specialized experts for each category (for example, LFP and $\text{Li}(\text{Ni}_x\text{Co}_y\text{Al}_{1-x-y})\text{O}_2$ (NCA) cathodes), selecting only those corresponding to the input battery. For temperature, treated as a continuous variable, experts are defined at discrete values and selected within ± 5 °C of the input (see *Methods*). For instance, an 18650 LFP/graphite cell cycled at 25 °C selects the LFP, graphite, 18650-format, and 20–30 °C temperature experts. Implementation-wise, hard encoder is realized via knowledge-based weight selection, viz., where initial expert weights associated with non-matching categories are filtered out, thereby enforcing physically meaningful routing. The selected experts operate in parallel to extract lifetime-relevant representations, and their outputs are adaptively aggregated through learned weights. It is worth noting that there can be multiple experts per category to allow fine-grained specialization for aging

factors that are not hard-coded (e.g., formation protocols and operating conditions), promoting accurate and transferable knowledge extraction across aging conditions. In this way, BatteryMoE alleviates the learning challenges of scarce and heterogeneous data by providing knowledge-guided inputs to the gate network and enforcing physically grounded expert selection. This design enables efficient capture and transfer of degradation knowledge across diverse battery systems. BatteryMoE also functions as a plugin module, compatible with various neural architectures by allowing different network types to serve as experts.

As shown in Fig. 2b, we implement the Pretrained Battery Transformer (PBT) using BatteryMoE modules as the core computational units. A “BatteryMoE feed-forward” module represents a mixture of expert networks selected according to BatteryMoE principles. In PBT, each charge–discharge cycle is first encoded via “BatteryMoE CyclePatch”¹², which tokenizes cycling data into cycle tokens. These embeddings are progressively refined through stacked BatteryMoE feed-forward layers with residual connections, producing higher-level representations that are passed to a transformer encoder, where standard feed-forward layers are replaced by BatteryMoE modules. The encoder output is then projected to predict battery cycle life.

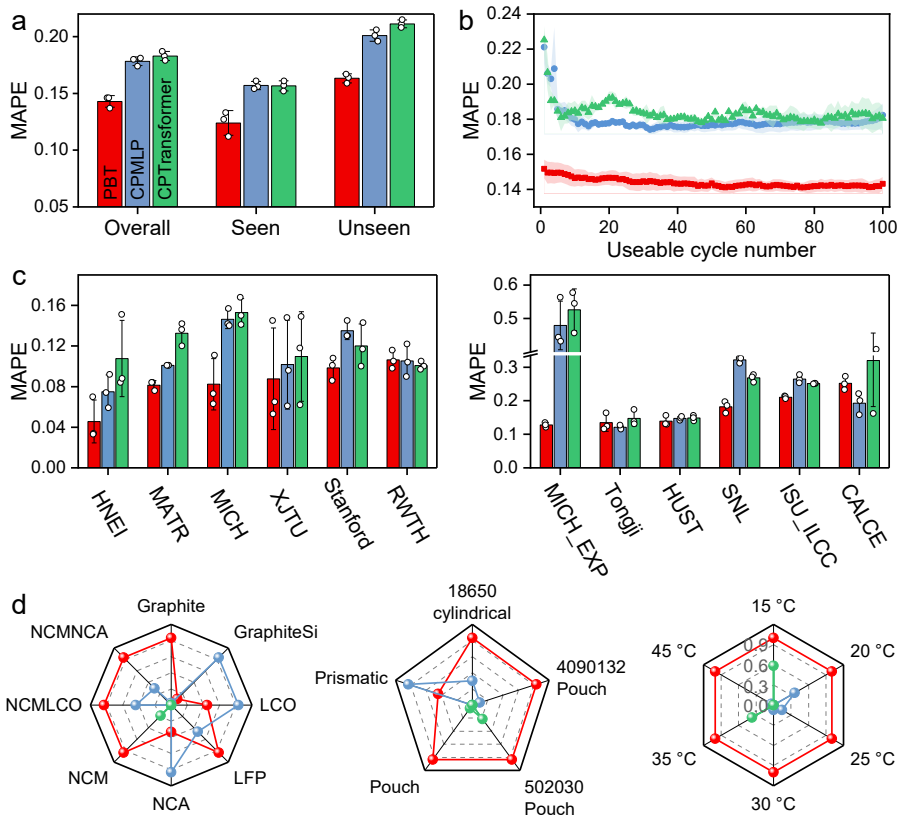


Fig. 3 | Evaluations of the comprehensiveness of battery lifetime knowledge in PBT. **a**, Overall model performance on the testing sets of the 13 pretrained LIB datasets. “Overall” denotes the average mean absolute percentage error (MAPE) across all batteries in the testing sets of the pretrained datasets. “Seen” and “Unseen” indicate the model performance on aging conditions that are covered or not covered by training and validation sets of the pretraining data, respectively. **b**, Model performance with increasing numbers of usable cycles. Shaded areas represent standard deviations across three independent runs. **c**, Model performance on the testing sets of individual pretraining datasets. Error bars indicate standard deviations of the mean. **d**, Model comparison by chemistry, physical format and operating temperature. Radial values show normalized MAPE computed as $1 - (x - \min) / (\max - \min)$, where x is the original MAPE and \min and \max are the best and worst MAPE within each category.

Evaluation of the comprehensiveness of battery life knowledge in PBT

To evaluate whether PBT can acquire universal representation for battery life data under conditions of data scarcity and heterogeneity, we pretrained it on 13 LIB datasets drawn from the collected database. These datasets comprise 837 batteries, spanning 426 aging conditions, 406 charge–discharge protocols, 8 operating temperatures, 13 chemical systems, and 5 physical formats, covering most commercial LIB chemistries (see Supplementary Table 1 for the chemistries covered by each dataset). Such unprecedentedly comprehensive battery life datasets offer a rigorous testbed for studying model’s capability of acquiring comprehensive battery life knowledge under data scarcity and heterogeneity.

Each dataset was randomly split into training, validation, and testing subsets with a 6:2:2 ratio. All model training was repeated three times with different random seeds and the data in the testing sets are used for evaluating model performance. Note that UL-PUR dataset has only 2 batteries after data preprocessing and thus has no testing set in this work. For all analysis, mean absolute percentage error (MAPE) is employed as the evaluation metric, because battery lifetime is significantly different in these datasets (see Supplementary Fig. 4 for battery life distributions of different datasets), ranging from 102 to 4999 cycles, and thus MAPE can avoid the bias created by different battery life scales. We compare PBT against two baselines (CPMLP and CPTransformer) identified as the leading models among 18 methods¹², including iTransformer⁷², PatchTST⁷³, MICN⁷⁴, and DLinear⁷⁵. Both baselines employ CyclePatch¹² to generate cycle-level embeddings but differ in how they model inter-cycle relationships. CPMLP uses multilayer perceptions to capture interactions across cycles, whereas CPTransformer leverages a Transformer encoder.

First, we compare the overall results of PBT with the leading baselines in Fig. 3a. As shown in Fig. 3a, PBT achieves the best performance with the overall MAPE as 0.143, surpassing the second-best model by 19.8%. To assess its robustness across data regimes, we further evaluate performance on seen (84) and unseen (81) aging

conditions—corresponding to in-distribution and out-of-distribution scenarios, respectively. According to Fig. 1a, PBT outperforms the second-best model by 20.8% on seen and 18.7% on unseen conditions, indicating that its superiority arises from consistent improvements on both in-distribution and out-of-distribution data. Moreover, we evaluate overall model performance with different useable cycle numbers and present the results in Fig. 3b. It shows that PBT maintains clear advantages under all settings, achieving up to 31.3% improvement when only the first cycle is available. Remarkably, PBT trained on a single cycle outperforms the second-best model using 100 cycles, suggesting that it can reduce data acquisition time by $\sim 99\%$ without sacrificing predictive accuracy.

Second, we evaluate model performance on each dataset and present the results in Fig. 3c. Since different datasets generally include different battery specifications. This evaluation reflects the battery life knowledge acquired in models for different battery specifications. It is observed that PBT achieves the best results in 9 out of 12 datasets with more than 20% improvements in 8 datasets. For 3 datasets (RWTH⁶⁶, Tongji⁶¹, CALCE^{59,60}) where PBT does not lead the performance, PBT still performs on a par with the best model on 2 (RWTH and Tongji) out of them. The observed deviation on the CALCE dataset is likely attributable to latent aging factors (e.g. electrolyte recipes, stacking stress and coating parameters) absent from public data. This absence limits the model's ability to fully resolve the underlying degradation progress. We posit that integrating such proprietary information, which is readily accessible to battery manufacturers, would resolve this discrepancy. These results indicate that PBT masters the most comprehensive battery life knowledge regarding various battery specifications.

Third, we evaluate if PBT acquires comprehensive battery life knowledge from 3 perspectives: chemistry, physical format and operation temperature, and conclude the results in Fig. 3d. We can observe that PBT is the best in 5 out of 8 chemistries, 4 out of 5 physical formats, 6 out of 6 operation temperatures. It is worth noting that PBT outperforms the second-best model by more than 13.7% in 15 aspects

among the 19 aspects. In short, PBT masters the most comprehensive battery life knowledge from all 3 perspectives.

Collectively, these results indicate that PBT has learned effective representations for diverse battery life data and basically lays the foundation for transferability for various downstream cycle life prediction applications.

PBT is transferable for batteries whose specifications are within pretraining data

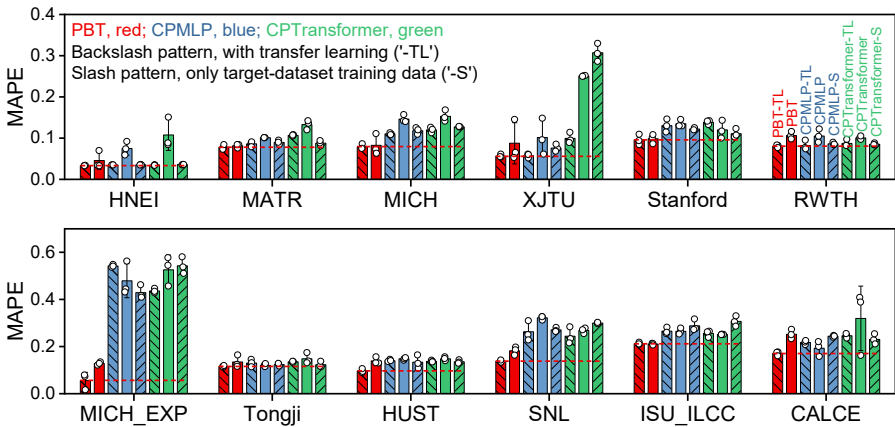


Fig. 4 | Transferability evaluation on 12 datasets in which battery specifications are within pretraining data. The dashed lines indicate the performance of PBT-TL as the visual reference. Transfer learning variants, denoted by the suffix –TL, are shown with the backslash pattern. Variants with the suffix –S represent models trained from scratch using only the target-dataset training data, and are shown with the slash pattern. Error bars indicate standard deviations across three independent runs.

To assess the utility of our PBT model for diverse cycle life prediction scenarios, we first evaluate its performance on batteries whose specifications are represented in the pretraining data. We adapt PBT to 12 datasets corresponding to various scenarios using two common transfer learning strategies⁵⁰ (see Supplementary Note 2): fine-tuning and adapter tuning. For a fair comparison, we apply identical transfer learning strategies to the CPMLP and CPTransformer, and report the best transfer learning results from each in Fig. 4. We additionally include (i) direct inference from the pretrained models and (ii) baseline

models trained from scratch on each target dataset to isolate the benefits of pretraining and transfer learning. PBT is also compared with BatLiNet¹¹, which is a recent work from the transfer learning research line in the battery lifetime prediction field (see Supplementary Note 3 for implementation details).

As shown in Fig. 4a, in comparison to CPMLP and CPTransformer as well as their transfer-learned variants, PBT-TL delivers the best results on all of 12 datasets, achieving a greater than 10% improvement on 8 of them, with an average performance gain of 22.02% over the best baseline. The 12 datasets span a series of critical application scenarios of cycle life prediction, including optimizations of fast-charge protocols (MATR^{14,15}), formation protocol analysis (Stanford⁵⁴), cycle life evaluation under various stress factors (MICH-EXP⁵⁶), and assessments across diverse operating conditions (Other datasets^{20,25,55,57,58,60-63,65,66}), indicating PBT's powerful versatility across various practical cases.

Notably, PBT-TL delivers larger gains when aging conditions become more heterogeneous under strong data scarcity. PBT-TL improves upon the best baseline by 3.85% on the HNEI dataset (9 training cells, 2 aging conditions), by 11.40% on the CALCE dataset (9 training cells, 4 aging conditions), and by a remarkable 86.95% on the highly challenging MICH_EXP⁵⁶ dataset, where all baselines fail when confronted with batteries with each belonging to a unique aging condition and only 7 batteries are provided for training. Intriguingly, while PBT does not initially lead on the CALCE dataset, it achieves state-of-the-art performance post-transfer learning. This reversal suggests that the model effectively leverages information from other datasets to enhance adaptation. This underscores the importance of capturing as comprehensive knowledge as possible for building an effective foundation model. Moreover, considering CPMLP/CPMLP-TL, CPTransformer/CPTransformer-TL, and PBT/PBT-TL all rely on the same pretraining data and transfer learning strategies, these results demonstrate that naively training neural models on diverse datasets does not suffice to learn extensively transferable representations for battery life data. PBT overcomes this limitation through the domain-

guided design of BatteryMoE, enabling effective knowledge transfer even under data scarcity and heterogeneity.

The importance of capturing such transferable representation is further underscored by the comparative transfer learning analysis. Although CPTransformer-TL outperforms CPTransformer on 10 datasets and CPMLP-TL outperforms CPMLP on 8 datasets, the frozen pretrained models (CPMLP, CPTransformer) and their variants with the target-dataset training data (namely, -S in Fig. 4) still achieve the second-best performance on 6 of the 12 datasets. This phenomenon suggests that transfer learning alone can provide incremental improvements, but state-of-the-art performance cannot be achieved unless the pretrained model already encodes sufficiently relevant aging knowledge. This is further supported by the results of BatLiNet on the 12 datasets (Supplementary Table 2). It reveals that BatLiNet fails to match PBT-TL on all datasets and produces $\text{MAPE} \geq 50\%$ on 5 datasets with only limited data or aging conditions substantially different from LFP/graphite cells—a trend also noted in its original paper¹¹. Considering that the original BatLiNet solely uses LFP/graphite cells as source domains, we additionally examine the performance of BatLiNet using the pretraining data of PBT as the source domains to remove the impact of pretraining data volume and diversity. As summarized in Supplementary Table 3, naively enlarging BatLiNet’s pretraining set in this way degrades its transfer performance on most datasets. This outcome highlights both the difficulty and the necessity of developing a foundation model that can effectively exploit diverse battery life data, rather than merely relying on larger volumes of heterogeneous pretraining samples.

In summary, these results demonstrate that PBT effectively captured transferable comprehensive battery degradation knowledge, enabling enhanced cycle life prediction for batteries whose specifications are covered by pretraining data. This capability positions PBT as a powerful tool with strong potential for a broad spectrum of practical cycle life prediction applications.

PBT is transferable for battery chemistries and designs beyond pretraining data

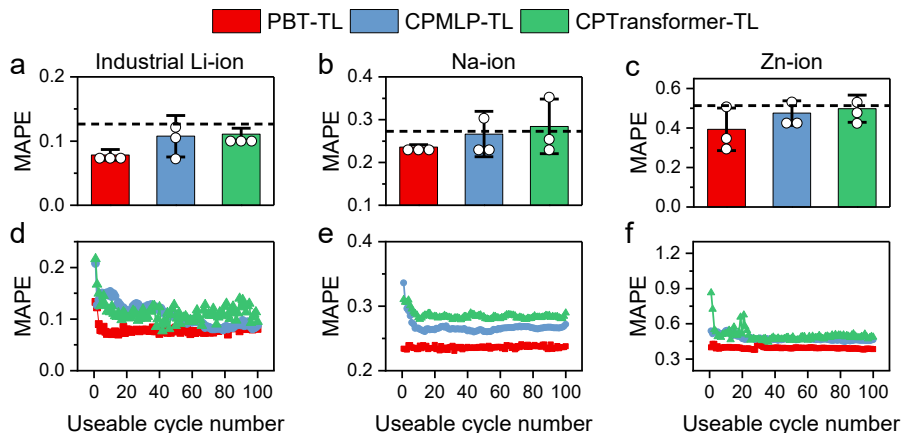


Fig. 5 | Transferability evaluation on batteries whose specifications are beyond pretraining data. **a–c**, Overall model performance on the industrial Li-ion (**a**), Na-ion (**b**), and Zn-ion battery (**c**) datasets. The dashed lines indicate the best results obtained by CPMLP and CPTransformer models trained from scratch using only the target-dataset training data. **d–f**, Model performance as a function of the number of useable cycles on the three datasets.

A critical test for battery lifetime foundation model is its ability to be transferred to new chemistries and designs not encountered during pretraining, a capability essential for accelerating the development of next-generation batteries. We therefore evaluate PBT on batteries whose fundamental specifications, including chemistry and industrial design, fall outside its pretraining distribution. Three datasets used here for this out-of-distribution assessment are the sodium-ion (Na-ion), zinc-ion (Zn-ion), and large-format industrial Li-ion datasets. The Na-ion and Zn-ion datasets probe PBT’s transferability to chemistries beyond LIBs, while the industrial dataset examines its useability for higher-capacity, large-format cells relevant to real-world industrial development of LIBs. Note that, for the industrial LIB dataset, we define predicted lifetime targets as the cycle number at which discharge capacity falls to 90% of nominal capacity, as most cells were not degraded to the 80% threshold. We evaluate PBT against the same baselines used in the previous evaluations on battery specifications that are covered by pretraining data. Direct inference with the pretrained

models yielded unsatisfactory results due to significant domain shifts and is omitted for clarity.

As shown in Fig. 5a–c, transfer-learned PBT (PBT-TL) achieves the lowest MAPE on all three datasets, outperforming the second-best model by 27.2%, 11.5%, and 17.2% for industrial Li-ion, Na-ion, and Zn-ion batteries, respectively. These results demonstrate PBT’s adaptability to both new chemistries and industrial-scale LIB development. Performance trends across varying numbers of usable cycles (Fig. 5d–f) further show that PBT-TL delivers consistent improvements over a broad early prediction period. Finally, we again notice that BatLiNet fails match PBT-TL (Supplementary Table 2 and Supplementary Table 3), indicating that PBT-TL’s gains stem from its ability to learn widely transferable representations from diverse battery life data.

Collectively, these findings confirm that PBT is highly transferable. The model can be successfully transferred to predict cycle life of batteries representing chemistries beyond LIB and industrial development of LIB, a cornerstone for accelerating the development and deployment of next-generation energy storage materials and systems.

Discussion and conclusions

This work introduces the foundation model PBT for advanced battery cycle life prediction on data of scarcity and heterogeneity. By infusing battery knowledge of degradation data into mixture-of-expert paradigm, we construct BatteryMoE. Built upon the proposed BatteryMoE module, the PBT effectively captures comprehensive and transferable lifetime knowledge from pretraining on 13 LIB datasets. It exhibits superior transferability across all 15 datasets, covering diverse application scenarios including various charge protocols, discharge protocols, operation temperatures, stress factors, formation protocols, industrial battery designs, and chemistries beyond LIBs. These capabilities position PBT as a robust tool for accelerating battery development and deployment across real-world applications.

Ablation and data-scaling analyses clarify the origin of PBT's effectiveness. Both the hard and soft encoders are essential for capturing underlying degradation behavior (Supplementary Fig. 1), enabling significant performance gains even with limited data. Moreover, incorporating BatteryMoE consistently improves results across data scales (Supplementary Fig. 5), with the encoded knowledge compensating for 33–50% of additional training data—highlighting its value in data-scarce regimes. Furthermore, the non-saturated scaling trend in Supplementary Fig. 5 scaling up pretraining data can further improve PBT's performance.

Importantly, BatteryMoE has a flexible framework for encoding battery knowledge. It is promising to further enhance model performance by hard-coding more aging factors (e.g., investigating the knowledge-based grouping of electrolytes and coating) and describing more aging factors using more powerful LLM in the LLM-based aging embedder in the future. Additionally, developing tailored transfer learning techniques for PBT may further enhance performance. For example, for large language models, prompt tuning^{76,77} enables efficient adaptation without modifying model parameters, and parameter-efficient fine-tuning methods such as LoRA⁷⁸ have also emerged as powerful alternatives to conventional fine-tuning, often achieving superior performance with far fewer trainable parameters. Exploring whether analogous, battery-specific transfer learning techniques can be developed for lifetime-prediction foundation models represents a promising direction for future work.

Moreover, beyond lifetime data collected from battery development and quality evaluations, future work will explore incorporating battery field data (e.g., data of energy storage systems⁴ and electric vehicles³) into PBT. Achieving this integration requires a unified lifetime metric that is broadly accepted, as batteries used in applications are typically operated under varying operating conditions with only partial charge-discharge data, making conventional cycle life calculations impractical. With such a metric, development and field data could complement one another, since both reflect degradation driven by the same degradation modes⁶⁸ even though the cycling data

patterns can be distinctly different. This integration could ultimately extend foundation models to encompass the entire battery lifecycle, from laboratory development to field operation. Notably, the underlying principle of PBT—decomposing heterogeneous data via domain knowledge—is broadly applicable to other domains in sciences and technologies (e.g., novel material discovery, solar cell life prediction, fatigue failure prediction, corrosion damage prediction, etc.), where data scarcity and heterogeneity persist.

Overall, this work highlights the potential of addressing data scarcity and heterogeneity in battery lifetime prediction through the development of tailored foundation models. Combined with advances in transfer learning strategies, this approach can accelerate progress in cycle life prediction, supporting faster battery development and deployment. We envision that machine learning models, particularly those that deeply integrate physical and electrochemical knowledge into their architectures, will become increasingly central to data-driven battery research. Such models are expected to overcome long-standing challenges in performance prediction, design optimization, and materials discovery, while extending their impact beyond the battery field.

Methods

The Pretrained Battery Transformer (PBT) is a battery-knowledge-encoded foundation model built upon the proposed BatteryMoE module. As illustrated in Fig. 2b, PBT consists of a BatteryMoE-CyclePatch layer, an BatteryMoE-intra-cycle encoder with L_1 layers, an BatteryMoE-inter-cycle encoder with L_2 layers, and a projection head. We first describe BatteryMoE, followed by the individual model components.

BatteryMoE. BatteryMoE is a mixture-of-experts layer that encodes battery knowledge through soft and hard encoders. Soft encoder (pink part in Fig. 2a) relies on knowledge-based pattern decomposition to discover aging factors that dominate cycling data patterns. These factors—spanning battery specifications, formation, and operation—are embedded into vectors as

$$\mathbf{e} = E_{ae}(\text{specification, formation, operation}), \quad (1)$$

where E_{ae} denotes an aging embedder and \mathbf{e} is the resulting vector representation. To construct a universal embedder applicable to arbitrary combinations of aging factors, we devise a large-language-model (LLM)-based aging embedder that produces token embeddings from a textual prompt describing the factors:

$$\bar{\mathbf{E}} = LLM(\text{prompt}), \quad (2)$$

$$\mathbf{e} = \text{lastValid}(\bar{\mathbf{E}}), \quad (3)$$

where prompt (see Supplementary Fig. 2) is a text description about the aging factors, $\bar{\mathbf{E}} \in \mathbb{R}^{L \times d_{LLM}}$ is the embedding of tokens obtained from the prompt, and $\mathbf{e} \in \mathbb{R}^{d_{LLM}}$ is the embedding of the last valid token in $\bar{\mathbf{E}}$. The embedding of the final valid token \mathbf{e} encodes the full context because of the LLM’s causal attention mechanism. In present study, Llama-3.1-8b-Instruct³⁶ is used as the LLM to comprehend the prompt. A nonlinear transformation further distills informative representations:

$$\hat{\mathbf{e}} = \text{LeakyReLU}(\mathbf{W}\mathbf{e} + \mathbf{b}), \quad (4)$$

where $\mathbf{W} \in \mathbb{R}^{d_{ff} \times d_{LLM}}$, $\mathbf{b} \in \mathbb{R}^{d_{ff}}$. The processed embedding $\hat{\mathbf{e}}$ is shared across BatteryMoE layers and used by a linear layer of individual BatteryMoE layer to determine expert weights as follows:

$$\mathbf{g} = [g_1, g_2, g_3, \dots, g_{K_s}] = \mathbf{W}_2 \hat{\mathbf{e}} + \mathbf{b}_2, \quad (5)$$

Where $\mathbf{W}_2 \in \mathbb{R}^{K_s \times d_{ff}}$, $\mathbf{b}_2 \in \mathbb{R}^{K_s}$ are learnable parameters and K_s is the number of specialized expert networks in a BatteryMoE layer.

Hard encoder (blue in Fig. 2a) operates through hard-coded routing rules within the mixture-of-experts layer. We define routing rules for four aging factors—cathode, anode, physical format, and operating temperature. Under this scheme, only the expert weights of corresponding expert networks are kept for modelling a given

battery:

$$\bar{\mathbf{g}} = \sigma(\mathbf{g}) \quad (6)$$

where $\sigma(\cdot)$ denotes the knowledge-based weight selection that sets irrelevant expert weights to zero. Specifically, for categorical factors (cathode, anode, and physical format), only expert networks corresponding to the selected category are used. For temperature, treated as a continuous variable, experts whose specialized temperatures fall within ± 5 °C of the input are selected. The resulting knowledge-informed expert weights $\bar{\mathbf{g}}$ is the output of Battery gate (Fig. 2a) and then used to aggregate outputs from expert networks:

$$\mathbf{M}^l = \sum_{i=1}^{K_g} F_i(\mathbf{M}^{l-1}) + \sum_{j=K_g+1}^{K_g+K_s} \bar{g}_j F_j(\mathbf{M}^{l-1}), \quad (7)$$

where K_g denote the number of general experts, respectively and $F_i(\cdot)$ is an expert network. This formulation makes BatteryMoE a plug-and-play component compatible with diverse expert architectures $F(\cdot)$. For brevity, in the following, we refer a BatteryMoE layer to $\text{BatteryMoE}(F(\cdot))$ when $F(\cdot)$ is used as the expert network architecture. To ensure effective expert specialization, each category is assigned one expert for up to 100 training batteries, with an additional expert added for every subsequent 100, following a round-to-nearest-hundred rule (e.g., 151 \rightarrow two experts, 101 \rightarrow still one). This adaptive allocation allows categories with larger training data to achieve finer-grained specialization through data-driven learning.

BatteryMoE-CyclePatch. Motivated by the previous success of CyclePatch¹², BatteryMoECyclePatch is first employed to patch the cycling data of each cycle into a token. Let $\mathbf{X}_{1:S} \in \mathbb{R}^{(300 \times S) \times 3}$ denote the voltage, current and capacity sequence of the first S cycles (each cycle has been resampled into 300 data points; see Supplementary Note 4). The process of BatteryMoECyclePatch can be described as follows:

$$[\mathbf{X}_1, \mathbf{X}_2, \mathbf{X}_3, \dots, \mathbf{X}_S] = \text{Segment}(\mathbf{X}_{1:S}), \quad (8)$$

$$\widehat{\mathbf{X}}_i = \text{BatteryMoE}\left(\text{Linear}(\text{Flatten}(\mathbf{X}_i))\right), \quad (9)$$

where $\mathbf{X}_i \in \mathbb{R}^{300 \times 3}$, $\text{Flatten}(\mathbf{X}_i) \in \mathbb{R}^{900}$, and $\text{Linear}(\cdot)$ is a linear layer that projects $\text{Flatten}(\mathbf{X}_i)$ to $\widehat{\mathbf{X}}_i \in \mathbb{R}^d$. In this vein, the recurring cycling data patterns are explicitly segmented into distinct tokens $\widehat{\mathbf{X}} = [\widehat{\mathbf{X}}_1, \widehat{\mathbf{X}}_2, \dots, \widehat{\mathbf{X}}_S]$.

BatteryMoE-Intra-cycle encoder. Following CyclePatch, an intra-cycle encoder is employed to deeply mine useful high-level representations for each cycle. This process of one intra-cycle encoder layer can be formulated as follows:

$$\mathbf{H}_i^l = \text{LN}\left(\text{BatteryMoE}\left(\text{FFN}(\mathbf{H}_i^{l-1})\right) + \mathbf{H}_i^{l-1}\right), \quad (10)$$

where $\text{LN}(\cdot)$ denotes the layer normalization⁷⁹, $\text{FFN}(\cdot)$ is a feed-forward network with GELU ⁸⁰ as the activation function, $\mathbf{H}_i^l \in \mathbb{R}^d$, and $\mathbf{H}_i^0 = \widehat{\mathbf{X}}_i$. After stacking this layer described in Equation (9) for L_1 layers, d features have been automatically extracted from each cycle. We then concatenate the cycle-token embeddings of S cycles producing \mathbf{H}^{L_1} , and feed \mathbf{H}^{L_1} to inter-cycle encoder for modeling critical information across cycles. For efficient batch operation, all \mathbf{H}^{L_1} is zero-padded to the length of 100, which is the largest useable cycle number for the model input. Therefore, $\mathbf{H}^{L_1} \in \mathbb{R}^{100 \times d}$.

BatteryMoE-Inter-cycle encoder. The inter-cycle encoder adopts a transformer⁸¹ encoder framework for modeling information across cycle tokens. First, positional encoding is used to incorporate position information into intra-cycle encoder output:

$$\bar{\mathbf{H}}^{L_1} = \text{PE}(\mathbf{H}^{L_1}) + \mathbf{H}^{L_1}, \quad (11)$$

where $\text{PE}(\cdot)$ is the positional encoding introduced in the original transformer paper⁸¹. Then, $\bar{\mathbf{H}}^{L_1}$ is input to the inter-cycle encoder, where the process of one layer is as follows:

$$\mathbf{P}^l = \text{LN}(\text{Attention}(\mathbf{P}^{l-1}, \mathbf{P}^{l-1}, \mathbf{P}^{l-1}) + \mathbf{P}^{l-1}), \quad (12)$$

$$\mathbf{U}^l = \text{LN}\left(\text{BatteryMoE}\left(\text{FFN}(\mathbf{P}^l)\right) + \mathbf{P}^l\right), \quad (13)$$

where $\text{Attention}(\cdot, \cdot, \cdot)$ is the self-attention operation, $\mathbf{P}^0 = \bar{\mathbf{H}}^{L_1}$, and $\mathbf{U}^l \in \mathbb{R}^{100 \times d}$ is the output of the l^{th} inter-cycle encoder layer. Note that attention mask is adopted to ignore padded tokens in $\text{Attention}(\cdot, \cdot, \cdot)$.

Projection head. After intra-cycle encoder and inter-cycle encoder, useful intra-cycle information and inter-cycle information are captured into \mathbf{U}^{L_2} . The last non-masked vector in \mathbf{U}^{L_2} is denoted by \mathbf{z} and is used as the input to projection head. The final prediction \hat{y} can be produced via a projection head that employs a mixture of linear layers:

$$\mathbf{g} = [g_1, g_2, g_3, \dots, g_{K_s}] = G(\mathbf{z}), \quad (14)$$

$$\hat{y} = \sum_{i=1}^5 F_i(\mathbf{z}) + \sum_{i=6}^{10} g_i F_i(\mathbf{z}), \quad (15)$$

Model optimization. The PBT is optimized by minimizing mean squared error $\mathcal{L} = (\hat{y} - y)^2$ using AdamW⁸² optimizer. The hyperparameters that lead to the best results on the validation set are selected. The searching range of hyperparameters and selected hyperparameters for pretraining PBT are listed in Supplementary Table 4. The effectiveness of the proposed BatteryMoE is also consolidated via ablation studies (Supplementary Fig. 1).

Data availability

All datasets used in the present study are publicly available, including CALCE^{59,60}, MATR^{14,15}, RWTH⁶⁶, HUST²⁰, Tongji⁶¹, Stanford⁵⁴, XJTU⁶², and ISU-ILCC⁵⁵. HNEI⁶³, SNL⁵⁸, MICH_EXP⁵⁶, MICH²⁵, and UL-PUR^{57,65} are hosted by BatteryArchive (<https://www.batteryarchive.org/>). The Zn-ion, Na-ion and industrial LIB datasets are hosted by BatteryLife¹². We used the preprocessing scripts from BatteryLife to process these datasets into a unified format to support model experiments reported in this article. The processed datasets are available at <https://github.com/Ruifeng-Tan/BatteryLife>.

Code availability

Code for this work is available at the following link: <https://github.com/Ruifeng-Tan/PBT>. The pretrained weights of PBT are available at <https://zenodo.org/records/17972780>.

Author contributions

T. Y. Zhang, J. Huang, R. Tan and J. Li conceived the idea. R. Tan designed the model and conducted the AI analysis with the help of X. Hong and J. Li. R. Tan, J. Huang and T. Y. Zhang wrote the paper with contributions from all authors. T. Y. Zhang and J. Huang managed the project and guided the research.

Acknowledgements

The authors acknowledge the financial support of the National Key R&D Program of China (No. 2023YFB2503600). This work is also supported by research grants from the National Natural Science Foundation of China (No. 92372109, No. 52207230, and No. 62206067) and the Guangzhou Municipal Science and Technology Project (No. 2024A04J4216). We acknowledge the supports from Wilson Tang Brilliant Energy Science and Technology Lab (BEST Lab) at the Hong Kong University of Science and Technology (Guangzhou).

Declarations

The authors declare no competing interests.

References

- 1 Huang, J., Boles, S. T. & Tarascon, J.-M. Sensing as the key to battery lifetime and sustainability. *Nature Sustainability* **5**, 194-204 (2022). <https://doi.org/10.1038/s41893-022-00859-y>
- 2 Tao, S. *et al.* Collaborative and privacy-preserving retired battery sorting for profitable direct recycling via federated machine learning. *Nature Communications* **14**, 8032 (2023). <https://doi.org/10.1038/s41467-023-43883-y>
- 3 Liu, H. *et al.* Multi-modal framework for battery state of health evaluation using open-source electric vehicle data. *Nature*

- Communications* **16**, 1137 (2025).
<https://doi.org/10.1038/s41467-025-56485-7>
- 4 Figgner, J. *et al.* Multi-year field measurements of home storage systems and their use in capacity estimation. *Nature Energy* **9**, 1438-1447 (2024). <https://doi.org/10.1038/s41560-024-01620-9>
- 5 Tan, R. *et al.* Forecasting battery degradation trajectory under domain shift with domain generalization. *Energy Storage Materials* **72**, 103725 (2024).
<https://doi.org/10.1016/j.ensm.2024.103725>
- 6 Miao, Y., Liu, L., Zhang, Y., Tan, Q. & Li, J. An overview of global power lithium-ion batteries and associated critical metal recycling. *Journal of Hazardous Materials* **425**, 127900 (2022).
<https://doi.org/https://doi.org/10.1016/j.jhazmat.2021.127900>
- 7 Fleischmann, J. *et al.* Battery 2030: Resilient, sustainable, and circular. *McKinsey & Company* **16**, 2023 (2023).
- 8 Zhang, N. *et al.* Rechargeable aqueous zinc-manganese dioxide batteries with high energy and power densities. *Nature Communications* **8**, 405 (2017). <https://doi.org/10.1038/s41467-017-00467-x>
- 9 Mi, J. *et al.* A ductile solid electrolyte interphase for solid-state batteries. *Nature* **647**, 86-92 (2025).
<https://doi.org/10.1038/s41586-025-09675-8>
- 10 Ruan, J. *et al.* Current collector interphase design for high-energy and stable anode-less sodium batteries. *Nature Sustainability* **8**, 530-541 (2025). <https://doi.org/10.1038/s41893-025-01545-5>
- 11 Zhang, H. *et al.* Battery lifetime prediction across diverse ageing conditions with inter-cell deep learning. *Nature Machine Intelligence* (2025). <https://doi.org/10.1038/s42256-024-00972-x>
- 12 Tan, R. *et al.* in *Proceedings of the 31st ACM SIGKDD Conference on Knowledge Discovery and Data Mining V.2* 5789–5800 (Association for Computing Machinery, Toronto ON, Canada, 2025).
- 13 Li, W., Zhang, H., van Vlijmen, B., Dechent, P. & Sauer, D. U. Forecasting battery capacity and power degradation with multi-task learning. *Energy Storage Materials* **53**, 453-466 (2022).
<https://doi.org/10.1016/j.ensm.2022.09.013>
- 14 Attia, P. M. *et al.* Closed-loop optimization of fast-charging protocols for batteries with machine learning. *Nature* **578**, 397-402 (2020). <https://doi.org/10.1038/s41586-020-1994-5>

- 15 Severson, K. A. *et al.* Data-driven prediction of battery cycle life before capacity degradation. *Nature Energy* **4**, 383-391 (2019). <https://doi.org/10.1038/s41560-019-0356-8>
- 16 Zhang, T., Tan, R., Zhu, P., Zhang, T.-Y. & Huang, J. Unlocking Ultrafast Diagnosis of Retired Batteries via Interpretable Machine Learning and Optical Fiber Sensors. *ACS Energy Letters* **10**, 862-871 (2025). <https://doi.org/10.1021/acseenergylett.4c03054>
- 17 Tao, S. *et al.* Immediate remaining capacity estimation of heterogeneous second-life lithium-ion batteries via deep generative transfer learning. *Energy & Environmental Science* **18**, 7413-7426 (2025). <https://doi.org/10.1039/d5ee02217g>
- 18 Tao, S. *et al.* Generative learning assisted state-of-health estimation for sustainable battery recycling with random retirement conditions. *Nature Communications* **15**, 10154 (2024). <https://doi.org/10.1038/s41467-024-54454-0>
- 19 Hu, J., Weng, L., Gao, Z. & Yang, B. State of Health Estimation and Remaining Useful Life Prediction of Electric Vehicles Based on Real-World Driving and Charging Data. *IEEE Transactions on Vehicular Technology* **72**, 382-394 (2023). <https://doi.org/10.1109/TVT.2022.3203013>
- 20 Ma, G. *et al.* Real-time personalized health status prediction of lithium-ion batteries using deep transfer learning. *Energy and Environmental Science* **15**, 4083-4094 (2022). <https://doi.org/10.1039/d2ee01676a>
- 21 Zhang, H. *et al.* in *12th International Conference on Learning Representations, ICLR 2024, May 7, 2024 - May 11, 2024.* (International Conference on Learning Representations, ICLR).
- 22 Rhyu, J. *et al.* Systematic feature design for cycle life prediction of lithium-ion batteries during formation. *Joule*, 101884 (2025). <https://doi.org/10.1016/j.joule.2025.101884>
- 23 Kim, M., Kim, I., Kim, J. & Choi, J. W. Lifetime Prediction of Lithium Ion Batteries by Using the Heterogeneity of Graphite Anodes. *ACS Energy Letters* **8**, 2946-2953 (2023). <https://doi.org/10.1021/acseenergylett.3c00695>
- 24 Sugiarto, L., Huang, Z. & Lu, Y.-C. Battery lifetime prediction using surface temperature features from early cycle data. *Energy & Environmental Science* **18**, 2511-2523 (2025). <https://doi.org/10.1039/d4ee05179c>

- 25 Weng, A. *et al.* Predicting the impact of formation protocols on battery lifetime immediately after manufacturing. *Joule* **5**, 2971-2992 (2021). <https://doi.org/10.1016/j.joule.2021.09.015>
- 26 Geslin, A. *et al.* Selecting the appropriate features in battery lifetime predictions. *Joule* **7**, 1956-1965 (2023). <https://doi.org/10.1016/j.joule.2023.07.021>
- 27 Tao, S. *et al.* Battery Cross-Operation-Condition Lifetime Prediction via Interpretable Feature Engineering Assisted Adaptive Machine Learning. *ACS Energy Letters* **8**, 3269-3279 (2023). <https://doi.org/10.1021/acsenergylett.3c01012>
- 28 Guo, N. *et al.* Semi-supervised learning for explainable few-shot battery lifetime prediction. *Joule* **8**, 1820-1836 (2024). <https://doi.org/10.1016/j.joule.2024.02.020>
- 29 Guha, A. & Patra, A. Online Estimation of the Electrochemical Impedance Spectrum and Remaining Useful Life of Lithium-Ion Batteries. *IEEE Transactions on Instrumentation and Measurement* **67**, 1836-1849 (2018). <https://doi.org/10.1109/TIM.2018.2809138>
- 30 Fei, Z., Zhang, Z., Yang, F. & Tsui, K.-L. A deep attention-assisted and memory-augmented temporal convolutional network based model for rapid lithium-ion battery remaining useful life predictions with limited data. *Journal of Energy Storage* **62**, 106903 (2023). <https://doi.org/10.1016/j.est.2023.106903>
- 31 Hsu, C.-W., Xiong, R., Chen, N.-Y., Li, J. & Tsou, N.-T. Deep neural network battery life and voltage prediction by using data of one cycle only. *Applied Energy* **306**, 118134 (2022). <https://doi.org/https://doi.org/10.1016/j.apenergy.2021.118134>
- 32 Cha, J. *et al.* in *35th Conference on Neural Information Processing Systems, NeurIPS 2021, December 6, 2021 - December 14, 2021*. 22405-22418 (Neural information processing systems foundation).
- 33 Kokkalis, K., Chronis, C., Politi, E., Dimitrakopoulos, G. & Varlamis, I. in *2024 IEEE 10th International Conference on Big Data Computing Service and Machine Learning Applications (BigDataService)*. 122-129.
- 34 Zhang, Z., Wang, Y., Ruan, X. & Zhang, X. Lithium-ion batteries lifetime early prediction using domain adversarial learning. *Renewable and Sustainable Energy Reviews* **208**, 115035 (2025). <https://doi.org/10.1016/j.rser.2024.115035>

- 35 Guo, D. *et al.* DeepSeek-R1 incentivizes reasoning in LLMs through reinforcement learning. *Nature* **645**, 633-638 (2025). <https://doi.org/10.1038/s41586-025-09422-z>
- 36 Grattafiori, A. *et al.* The llama 3 herd of models. *arXiv preprint arXiv:2407.21783* (2024).
- 37 Devlin, J., Chang, M.-W., Lee, K. & Toutanova, K. 4171-4186 (Association for Computational Linguistics).
- 38 Peters, M. E. *et al.* in *2018 Conference of the North American Chapter of the Association for Computational Linguistics: Human Language Technologies, NAACL HLT 2018, June 1, 2018 - June 6, 2018*. 2227-2237 (Association for Computational Linguistics (ACL)).
- 39 Achiam, J. *et al.* Gpt-4 technical report. *arXiv preprint arXiv:2303.08774* (2023).
- 40 Brown, T. B. *et al.* in *34th Conference on Neural Information Processing Systems, NeurIPS 2020, December 6, 2020 - December 12, 2020*. Apple; et al.; Microsoft; PDT Partners; Sony; Tenstorrent (Neural information processing systems foundation).
- 41 Dai, D. *et al.* in *62nd Annual Meeting of the Association for Computational Linguistics, ACL 2024, August 11, 2024 - August 16, 2024*. 1280-1297 (Association for Computational Linguistics (ACL)).
- 42 Saini, S. S. & Rawat, P. in *2022 IEEE International Conference on Distributed Computing and Electrical Circuits and Electronics (ICDCECE)*. 1-4.
- 43 Hou, Q. *et al.* Vision Permutator: A Permutable MLP-Like Architecture for Visual Recognition. *IEEE Transactions on Pattern Analysis and Machine Intelligence* **45**, 1328-1334 (2023). <https://doi.org/10.1109/TPAMI.2022.3145427>
- 44 Radford, A. *et al.* in *38th International Conference on Machine Learning, ICML 2021, July 18, 2021 - July 24, 2021*. 8748-8763 (ML Research Press).
- 45 Redmon, J., Divvala, S., Girshick, R. & Farhadi, A. in *29th IEEE Conference on Computer Vision and Pattern Recognition, CVPR 2016, June 26, 2016 - July 1, 2016*. 779-788 (IEEE Computer Society).
- 46 Liang, Y. *et al.* in *30th ACM SIGKDD Conference on Knowledge Discovery and Data Mining, KDD 2024, August 25, 2024 - August 29, 2024*. 6555-6565 (Association for Computing Machinery).

- 47 Bommasani, R. On the opportunities and risks of foundation models. *arXiv preprint arXiv:2108.07258* (2021).
- 48 Qing, P. *et al.* 20511-20523 (Association for Computational Linguistics).
- 49 Zhao, C. *et al.* Learning Domain Invariant Prompt for Vision-Language Models. *IEEE Trans Image Process* **33**, 1348-1360 (2024). <https://doi.org/10.1109/TIP.2024.3362062>
- 50 Zheng, H. *et al.* Learning from models beyond fine-tuning. *Nature Machine Intelligence* **7**, 6-17 (2025). <https://doi.org/10.1038/s42256-024-00961-0>
- 51 Jiang, J., Zuo, Z., Wu, G., Jiang, K. & Liu, X. A Survey on All-in-One Image Restoration: Taxonomy, Evaluation and Future Trends. *IEEE Transactions on Pattern Analysis and Machine Intelligence* **47**, 11892-11911 (2025). <https://doi.org/10.1109/TPAMI.2025.3598132>
- 52 Zeng, F., Zhu, F., Guo, H., Zhang, X.-Y. & Liu, C.-L. 12137-12152 (Association for Computational Linguistics).
- 53 Dosovitskiy, A. *et al.* in *9th International Conference on Learning Representations, ICLR 2021, May 3, 2021 - May 7, 2021*. Amazon; DeepMind; et al.; Facebook AI; Microsoft; OpenAI (International Conference on Learning Representations, ICLR).
- 54 Cui, X. *et al.* Data-driven analysis of battery formation reveals the role of electrode utilization in extending cycle life. *Joule* **8**, 3072-3087 (2024). <https://doi.org/https://doi.org/10.1016/j.joule.2024.07.024>
- 55 Li, T., Zhou, Z., Thelen, A., Howey, D. A. & Hu, C. Predicting battery lifetime under varying usage conditions from early aging data. *Cell Reports Physical Science* **5**, 101891 (2024). <https://doi.org/10.1016/j.xcrp.2024.101891>
- 56 Mohtat, P., Lee, S., Siegel, J. B. & Stefanopoulou, A. G. Reversible and Irreversible Expansion of Lithium-Ion Batteries Under a Wide Range of Stress Factors. *Journal of The Electrochemical Society* **168**, 100520 (2021). <https://doi.org/10.1149/1945-7111/ac2d3e>
- 57 Juarez-Robles, D., Jeevarajan, J. A. & Mukherjee, P. P. Degradation-Safety Analytics in Lithium-Ion Cells: Part I. Aging under Charge/Discharge Cycling. *Journal of The Electrochemical Society* **167**, 160510 (2020). <https://doi.org/10.1149/1945-7111/abc8c0>

- 58 Preger, Y. *et al.* Degradation of Commercial Lithium-Ion Cells as a Function of Chemistry and Cycling Conditions. *Journal of The Electrochemical Society* **167**, 120532 (2020).
<https://doi.org/10.1149/1945-7111/abae37>
- 59 He, W., Williard, N., Osterman, M. & Pecht, M. Prognostics of lithium-ion batteries based on Dempster–Shafer theory and the Bayesian Monte Carlo method. *Journal of Power Sources* **196**, 10314-10321 (2011).
<https://doi.org/10.1016/j.jpowsour.2011.08.040>
- 60 Xing, Y., Ma, E. W. M., Tsui, K.-L. & Pecht, M. An ensemble model for predicting the remaining useful performance of lithium-ion batteries. *Microelectronics Reliability* **53**, 811-820 (2013).
<https://doi.org/https://doi.org/10.1016/j.microrel.2012.12.003>
- 61 Zhu, J. *et al.* Data-driven capacity estimation of commercial lithium-ion batteries from voltage relaxation. *Nature Communications* **13**, 2261 (2022).
<https://doi.org/10.1038/s41467-022-29837-w>
- 62 Wang, F., Zhai, Z., Zhao, Z., Di, Y. & Chen, X. Physics-informed neural network for lithium-ion battery degradation stable modeling and prognosis. *Nature Communications* **15**, 4332 (2024).
<https://doi.org/10.1038/s41467-024-48779-z>
- 63 Devie, A., Baure, G. & Dubarry, M. Intrinsic Variability in the Degradation of a Batch of Commercial 18650 Lithium-Ion Cells. *Energies* **11**, 1031 (2018).
- 64 Lin, M. *et al.* Lithium-ion battery degradation trajectory early prediction with synthetic dataset and deep learning. *Journal of Energy Chemistry* **85**, 534-546 (2023).
<https://doi.org/https://doi.org/10.1016/j.jechem.2023.06.036>
- 65 Juarez-Robles, D., Azam, S., Jeevarajan, J. A. & Mukherjee, P. P. Degradation-Safety Analytics in Lithium-Ion Cells and Modules: Part III. Aging and Safety of Pouch Format Cells. *Journal of The Electrochemical Society* **168**, 110501 (2021).
<https://doi.org/10.1149/1945-7111/ac30af>
- 66 Li, W. *et al.* One-shot battery degradation trajectory prediction with deep learning. *Journal of Power Sources* **506**, 230024 (2021).
<https://doi.org/10.1016/j.jpowsour.2021.230024>
- 67 Huang, X. *et al.* Physics-informed mixture of experts network for interpretable battery degradation trajectory computation amid

- second-life complexities. *arXiv preprint arXiv:2506.17755* (2025).
- 68 Birkel, C. R., Roberts, M. R., McTurk, E., Bruce, P. G. & Howey, D. A. Degradation diagnostics for lithium ion cells. *Journal of Power Sources* **341**, 373-386 (2017).
<https://doi.org/10.1016/j.jpowsour.2016.12.011>
- 69 Cai, W. *et al.* A Survey on Mixture of Experts in Large Language Models. *IEEE Transactions on Knowledge and Data Engineering*, 1-20 (2025). <https://doi.org/10.1109/tkde.2025.3554028>
- 70 Li, Q. *et al.* The critical importance of stack pressure in batteries. *Nature Energy* (2025). <https://doi.org/10.1038/s41560-025-01820-x>
- 71 Liu, C. *et al.* Air-stable Li₅FeO₄ additive enabled by carbon coating for energy-dense lithium-ion batteries. *Nature Communications* **16**, 7694 (2025).
<https://doi.org/10.1038/s41467-025-62418-1>
- 72 Liu, Y. *et al.* in *12th International Conference on Learning Representations, ICLR 2024, May 7, 2024 - May 11, 2024*. (International Conference on Learning Representations, ICLR).
- 73 Nie, Y., Nguyen, N. H., Sinthong, P. & Kalagnanam, J. in *11th International Conference on Learning Representations, ICLR 2023, May 1, 2023 - May 5, 2023*. Baidu; DeepMind; et al.; Google Research; Huawei; Meta AI (International Conference on Learning Representations, ICLR).
- 74 Wang, H. *et al.* in *11th International Conference on Learning Representations, ICLR 2023, May 1, 2023 - May 5, 2023*. Baidu; DeepMind; et al.; Google Research; Huawei; Meta AI (International Conference on Learning Representations, ICLR).
- 75 Zeng, A., Chen, M., Zhang, L. & Xu, Q. in *37th AAAI Conference on Artificial Intelligence, AAAI 2023, February 7, 2023 - February 14, 2023*. 11121-11128 (AAAI Press).
- 76 Lester, B., Al-Rfou, R. & Constant, N. in *2021 Conference on Empirical Methods in Natural Language Processing, EMNLP 2021, November 7, 2021 - November 11, 2021*. 3045-3059 (Association for Computational Linguistics (ACL)).
- 77 Liu, X. *et al.* in *60th Annual Meeting of the Association for Computational Linguistics, ACL 2022, May 22, 2022 - May 27, 2022*. 61-68 (Association for Computational Linguistics (ACL)).

- 78 Hu, E. *et al.* in *10th International Conference on Learning Representations, ICLR 2022, April 25, 2022 - April 29, 2022*. ByteDance; et al.; Meta AI; Microsoft; Qualcomm; Sea AI Lab (International Conference on Learning Representations, ICLR).
- 79 Ba, J. L. Layer normalization. *arXiv preprint arXiv:1607.06450* (2016).
- 80 Hendrycks, D. Gaussian Error Linear Units (Gelus). *arXiv preprint arXiv:1606.08415* (2016).
- 81 Vaswani, A. *et al.* in *31st Annual Conference on Neural Information Processing Systems, NIPS 2017, December 4, 2017 - December 9, 2017*. 5999-6009 (Neural information processing systems foundation).
- 82 Loshchilov, I. & Hutter, F. in *7th International Conference on Learning Representations, ICLR 2019, May 6, 2019 - May 9, 2019*. (International Conference on Learning Representations, ICLR).

Supplementary Information

Pretrained Battery Transformer (PBT): A battery life prediction foundation model

Ruifeng Tan^{1,2}, Weixiang Hong¹, Jia Li^{3*}, Jiaqiang Huang^{1,4,5*} and Tong-Yi Zhang^{6*}

¹Guangzhou Municipal Key Laboratory of Materials Informatics and Sustainable Energy and Environment Thrust, The Hong Kong University of Science and Technology (Guangzhou), Nansha, Guangzhou, 511400, Guangdong, P.R. China.

²Department of Computer Science & Engineering, The Hong Kong University of Science and Technology, Clear Water Bay, Kowloon, 999077, Hong Kong, P.R. China.

³Guangzhou Municipal Key Laboratory of Materials Informatics and Data Science and Analytics Thrust, The Hong Kong University of Science and Technology (Guangzhou), Nansha, Guangzhou, 511400, Guangdong, P.R. China.

⁴Academy of Interdisciplinary Studies, The Hong Kong University of Science and Technology, Clear Water Bay, Kowloon, 999077, Hong Kong, P.R. China.

⁵Guangzhou HKUST Fok Ying Tung Research Institute, Nansha District, Guangzhou, 511458, Guangdong, P.R. China.

⁶Material Genome Institute, Shanghai University, 333 Nanchen Road, Shanghai 200444, P.R. China; Guangzhou Municipal Key Laboratory of Materials Informatics, Advanced Materials Thrust, and Sustainable Energy and Environment Thrust, The Hong Kong University of Science and Technology (Guangzhou), Nansha, Guangzhou, 511400, Guangdong, P.R. China.

*Corresponding authors.

E-mails: jjalee@ust.hk; seejhuang@hkust-gz.edu.cn; mezhangt@hkust-gz.edu.cn

Supplementary Notes

Supplementary Note 1. Details of ageing conditions of the five batteries shown in Fig. 1c

The file names (the names are sourced from the raw files) and ageing conditions as well as cycle life of the five batteries shown in Fig. 1c are as follows:

1. **HNEI_18650_NMC_LCO_25C_0-100_0.5-1.5C_e**: The cycle life is 259. This is a lithium-ion battery (LIB) in a format of 18650 cylindrical battery. Its positive electrode is a mixture of LiCoO_2 (LCO) and $\text{LiNi}_{0.4}\text{Co}_{0.4}\text{Mn}_{0.2}\text{O}_2$ (NCM442). Its negative electrode is graphite. The electrolyte formula is unknown. The battery manufacturer is LG Chemical Limited. The working ambient temperature of this battery is 25 degrees Celsius. The cycling consists of three different strategies. For 1st to 10th cycles, the battery was charged at a constant current of 0.5 C until reaching 4.3 V, then was discharged at a constant current of 0.5 C until reaching 3 V. The cycling state-of-charge of this battery ranges from 0% to 100%.
2. **MICH_05C_pouch_NMC_-5C_0-100_1.5-1.5C**: The cycle life is 325. This is a LIB in a format of pouch battery. Its positive electrode is $\text{Li}(\text{Ni}_{0.33}\text{Co}_{0.33}\text{Mn}_{0.33})\text{O}_2$ (NCM111). Its negative electrode is graphite. The electrolyte formula consists of 1M LiPF_6 salt in solvents of ethylene carbonate (EC) and ethyl methyl carbonate (EMC) with a ratio of 3:7. The battery manufacturer is LISHEN. The nominal capacity is 5.0 Ah. The working ambient temperature of this battery is -5 degrees Celsius. In the cycling, the battery was charged at a constant current of 1.5 C until reaching 4.2 V, and then 4.2 V was sustained until the current dropped to 0.02 C. The battery was then discharged at a constant current of 1.5 C until reaching 3.0 V. The cycling state-of-charge of this battery ranges from 0% to 100%.
3. **XJTU_2C_battery-8**: The cycle life is 420. This is a LIB in a format of 18650 cylindrical battery. Its positive electrode is $\text{Li}(\text{Ni}_{0.5}\text{Co}_{0.2}\text{Mn}_{0.3})\text{O}_2$ (NCM523). Its negative electrode is graphite. The electrolyte formula is unknown. The battery manufacturer is LISHEN. The nominal capacity is 2 Ah. The working ambient temperature of this battery is 20 degrees Celsius. In the cycling, the battery was charged at a constant current of 2 C until reaching 4.2 V, and then 4.2 V was sustained until the current dropped to 0.05 C. And then rest for 5 minutes. The battery was then discharged at a constant current of 1 C until reaching 2.5 V, and then rest for 5 minutes. The cycling state-of-charge of this battery ranges from 0% to 100%.
4. **RWTH_010, MATR_b1c2**: The cycle life is 696. This is a LIB in a format of 18650 cylindrical battery. Its positive electrode is NCM and negative electrode is carbon. The electrolyte formula is unknown. The battery manufacturer is

Sanyo/Panasonic. The nominal capacity is 3 Ah. The working ambient temperature of this battery is 25 degrees Celsius. In the cycling, the battery was discharged at a constant current of 2 C until reaching 3.5 V. The battery was then charged at a constant current of 2 C until reaching 3.9 V. The cycling state-of-charge of this battery ranges from 20% to 80%.

5. **MATR_b1c2:** The cycle life is 2237. This is a LIB in a format of 18650 cylindrical battery. Its positive electrode is a lithium iron phosphate (LiFePO_4). Its negative electrode is graphite. The electrolyte formula is unknown. The battery manufacturer is A123 system. The nominal capacity is 1.1 Ah. Operating condition: The working history of this battery is just after formation. The working ambient temperature of this battery is 30 degrees Celsius. In the cycling, the battery was charged at a constant current of 3.6 C to 80% state-of-charge (SOC) until reaching 3.6 V. The battery was then discharged at a constant current of 4 C until reaching 2 V. The cycling state-of-charge of this battery ranges from 0% to 100%.

Supplementary Note 2. Implementation details of transfer learning methods

In this work, we utilized two kinds of transfer learning methods: fine-tuning and adapter tuning¹. For fine-tuning, all parameters of the pretrained model are updated using (i) a learning rate selected from 10^{-5} to 10^{-4} , (ii) a batch size chosen from [4,8,16,32,64,128,256], (iii) a weight decay in the AdamW² optimizer selected from [0,10.0], and (iv) a dropout rate from [0.0,0.05,0.15,0.25].

For adapter tuning, we insert adapter layers after the first N layers of the pretrained model. Each adapter transforms the input as:

$$\hat{x} = W_2 \text{GELU}(W_1 \text{LN}(x) + b_1) + b_2, \quad (1)$$

where $x \in \mathbb{R}^d$, $W_1 \in \mathbb{R}^{d \times d_a}$ and $b_1 \in \mathbb{R}^{d_a}$ are learnable parameters, $W_2 \in \mathbb{R}^{d_a \times d}$ and $b_2 \in \mathbb{R}^d$ are learnable parameters, $\text{LN}(\cdot)$ denotes the layer normalization³, and d_a denotes the adapter embedding dimension. We tune N from [1,12] (PBT contains 12 encoder layers), batch size from [4,8,16,32,64,128,256], learning rate from $[5 \times 10^{-6}, 10^{-3}]$, weight decay from [0,10.0], dropout rate from [0.0,0.05,0.15,0.25], and d_a from [1,128]. Final hyperparameters for both transfer learning methods are selected based on validation performance.

Supplementary Note 3. Implementation details of BatLiNet

The BatLiNet is reproduced using the official code available at <https://codeocean.com/capsule/2426768/tree/v2>.

We used the same dataset splits of the present study for training BatLiNet and tuned the hyperparameters of it to facilitate fair comparisons. For the hyperparameters, we

selected a dropout from $[0, 0.5]$, and a batch size chosen from $[32, 64, 128]$. Additionally, we tune two hyperparameters as follows:

1. `diff_base`: Let x_i denotes the features of the i^{th} cycle. BatLiNet computes $x_i - x_{diff_base}$ as the features of i^{th} cycle. We selected `diff_base` from $[10, 15, 20]$.
2. `alpha`: BatLiNet relies on an intra-cell learning branch and inter-cell learning branch, and alpha is a hyperparameter used to balance the loss and prediction from the two branches: $\mathcal{L} = \alpha\mathcal{L}_{intra} + (1 - \alpha)\mathcal{L}_{inter}$ and $\hat{y} = \alpha\hat{y}_{intra} + (1 - \alpha)\hat{y}_{inter}$. We selected `alpha` from $[0, 0.2, 0.5, 0.8]$.

To specify the reference batteries (source domains) for transfer learning in BatLiNet, two configurations were considered:

1. LiFePO4 source domain (aligned with the original implementation): Reference batteries were randomly sampled from LiFePO4 cells in the MATR, HUST, and SNL datasets.
2. Broader and more heterogeneous corpus: Reference batteries were randomly sampled from 13 datasets (CALCE, HNEI, MATR, SNL, UL_PUR, MICH_EXP, MICH, HUST, Tongji, Stanford, ISU_ILCC, and XJTU datasets), covering diverse ageing conditions.

All experiments were executed three times with distinct random seeds. Performance is reported as mean \pm standard deviation and is summarized in Supplementary Table 2 and Supplementary Table 3. We note that BatLiNet relies on a fixed number of collected cycles for lifetime prediction. Given the substantial computational overhead of BatLiNet (validation on 15 datasets costed two months using 16 RTX 4090 GPUs), we restricted our evaluation to the version utilizing the first 20 cycles as input. For the BatLiNet configuration using the 13 datasets as source domains, we reproduced its performance on only 9 downstream datasets because of the time-intensive training procedure.

Supplementary Note 4. Further details of BatteryMoE-CyclePatch

Given the voltage and current time series, we compute the capacity for a given charging/discharging period using the Coulomb counting method:

$$Q = \int_{t_1}^{t_2} |I| dt, \quad (2)$$

where t_1 is the start time of charging/discharging, and t_2 is any time within the same charging/discharging period. This procedure provides the corresponding capacity values. Because different cycles contain different numbers of sampled points, we

resample each cycle to 300 data points, with 150 points for charging and 150 points for discharging. Each point includes voltage, current, and capacity records. For consistency across datasets, voltage is expressed in volts, current in C-rate, and capacity in ampere-hours (Ah).

Supplementary Tables

Supplementary Table 1. The chemistries of the collected 16 datasets in this study.

Dataset	Positive electrode	Negative electrode	Electrolyte
CALCE	LiCoO ₂ (LCO)	Graphite	Unknown
MATR	LiFePO ₄ (LFP)	Graphite	Unknown
HUST	LFP	Graphite	Unknown
HNEI	LCO/ (NCM442)	LiNi _{0.4} Co _{0.4} Mn _{0.2} O ₂ Graphite	Unknown
RWTH	NCM	Carbon	Unknown
SNL	LFP/ LiNi _{0.81} Co _{0.14} Al _{0.05} O ₂ (NCA811405)/ LiNi _{0.84} Co _{0.1} Mn _{0.06} O ₂ (NCM840610)	Graphite	Unknown
UL-PUR	NCA801505	Graphite	Unknown
MICH	NCM111	Graphite	1.0 M LiPF ₆ Salt, EC:EMC(3:7) and 2wt% VC
MICH-EXP	NCM111	Graphite:PVDF (95:5)	1 M LiPF ₆ with 2% EC:EMC (3:7)
Stanford	NCM523	Artificial Graphite	1 M LiPF ₆ in EC/EMC/DMC (1 : 1 : 1 by volume) solvent with 2% VC (by weight) additive
Tongji	NCA861103/ NCM831107 /42 wt.% LiNiCoMnO ₂ blended with 58 wt.% LiNiCoAlO ₂	Graphite/ wt.% Si Graphite	2 non-aqueous + solution with LiPF ₆
XJTU	NCM523	Graphite	Unknown
ISU-ILCC	NCM	Graphite	Unknown
Zn-ion	MnO ₂	Zinc	2 M ZnSO ₄ in H ₂ O with multiple additives
Na-ion	Unknown	Unknown	Unknown
CALB	NCM	Graphite	Unknown

Supplementary Table 2. The comparison between PBT and BatLiNet⁴ on testing sets of the collected 15 datasets. The “Imp” denotes the relative improvement of PBT-TL over BatLiNet. Both models have only the first 20 cycles as the input. The Industrial Li-ion, Na-ion and Zn-ion battery datasets have 3 random splits and thus the training battery number for the 3 random splits are all reported. The best results are highlighted.

Dataset	PBT-TL	BatLiNet	Imp	Training battery number
HNEI	0.033±0.002	1.419±0.136	97.65%	9
MATR	0.077±0.006	0.161±0.031	51.85%	102
MICH	0.084±0.007	0.353±0.050	76.01%	24
XJTU	0.055±0.010	1.408±0.107	96.04%	15
Stanford	0.094±0.012	0.104±0.008	9.26%	25
RWTH	0.082±0.003	0.175±0.135	53.14%	30
MICH_EXP	0.061±0.035	1.16±0.175	94.71%	7
Tongji	0.134±0.002	0.195±0.018	31.39%	66
HUST	0.098±0.014	0.121±0.003	18.95%	47
SNL	0.143±0.006	1.836±0.428	92.17%	30
ISU_ILCC	0.210±0.007	0.857±0.054	75.41%	144
CALCE	0.191±0.056	1.22±0.712	84.39%	9
Industrial Li-ion	0.090±0.012	1.80±0.15	94.98%	17, 17, 17
Na-ion	0.237±0.004	1.85±0.243	87.16%	20, 20, 20
Zn-ion	0.389±0.113	1.62±0.086	76.11%	58, 57, 55

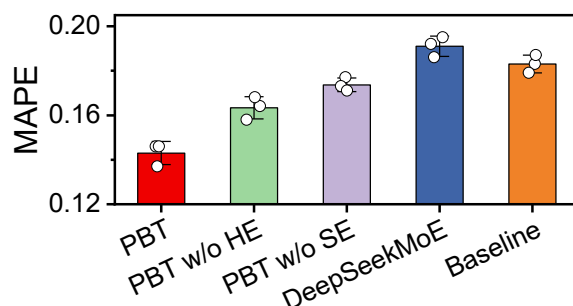
Supplementary Table 3. The comparison between PBT and BatLiNet⁴ on testing sets of the collected 15 datasets. In this table, the BatLiNet-Large uses the pretraining data of PBT as the source domains. BatLiNet only uses LFP/graphite cells as source domains. Due to the time-intensive training procedure, we reproduced the performance of BatLiNet-Large on only 9 downstream datasets. The “Imp” denotes the relative improvement of PBT-TL over BatLiNet-Large. Both models have only the first 20 cycles as the input. The Industrial Li-ion, Na-ion and Zn-ion battery datasets have 3 random splits and thus the training battery number for the 3 random splits are all reported. The best results are highlighted.

Dataset	PBT-TL	BatLiNet-Large	BatLiNet	Imp	Training battery number
HNEI	0.033±0.002	0.046±0.010	1.419±0.136	28.26%	9
MATR	0.077±0.006	-	0.161±0.031	-	102
MICH	0.084±0.007	-	0.353±0.050	-	24
XJTU	0.055±0.010	-	1.408±0.107	-	15
Stanford	0.094±0.012	-	0.104±0.008	-	25
RWTH	0.082±0.003	-	0.175±0.135	-	30
MICH_EXP	0.061±0.035	0.967±0.149	1.16±0.175	93.69%	7
Tongji	0.134±0.002	0.308±0.010	0.195±0.018	56.49%	66
HUST	0.098±0.014	0.129±0.005	0.121±0.003	24.03%	47
SNL	0.143±0.006	-	1.836±0.428	-	30
ISU_ILCC	0.210±0.007	0.481±0.024	0.857±0.054	56.34%	144
CALCE	0.191±0.056	11.163±12.171	1.22±0.712	98.28%	9
Industrial Li-ion	0.090±0.012	1.524±1.052	1.80±0.15	94.09%	17, 17, 17
Na-ion	0.237±0.004	1.645±0.359	1.85±0.243	85.59%	20, 20, 20
Zn-ion	0.389±0.113	1.383±0.200	1.62±0.086	71.87%	58, 57, 55

Supplementary Table 4. Selected hyperparameters used in model training. The table lists the key hyperparameters and their optimized values used for the Pretrained Battery Transformer (PBT). The notation d_{ff} and d follow the definitions in the Methods section.

Hyperparameters	Searching range	Selected value
Learning rate	10^{-3} - 10^{-5}	2.5×10^{-5}
Batch size	128, 256	256
The number of attention heads	4, 8, 16	8
The number of encoder layers	1-12	2
The number of decoder layers	1-12	10
d_{ff} (see Methods)	256, 512	512
Embedding dimension of CyclePatch (d , see Methods)	32, 64, 128, 256	128
Dropout rate	0.0, 0.05, 0.25	0.05
Embedding dimension of FFN	64, 128, 256	128

Supplementary Figures



Supplementary Figure 1. Ablation studies evaluating the efficacy of the proposed hard encoder (HE) and soft encoder (SE). PBT denotes the proposed Pretrained Battery Transformer. “w/o” denotes the exclusion of a technique; for example, “w/o HE” refers to the removal of hard encoder. DeepSeekMoE⁵ is shown as a reference model naively applying a generic language MoE to battery data. Baseline corresponds to the PBT without BatteryMoE.

a

Task description: The target the number of cycles until the battery’s discharge capacity reaches [x]% of its nominal capacity. The discharge capacity is calculated under the described operating condition. Please directly output the target of the battery based on the provided data.

Battery specifications: The data comes from a [x]-ion battery in a format of [x]. Its positive electrode is [x]. Its negative electrode is [x]. The electrolyte formula is [x]. The battery manufacturer is [x]. The nominal capacity is [x].

Operating condition: [If the formation protocol is available, include it here. Otherwise, indicate that the battery’s operating history begins immediately after formation.]. The working ambient temperature of this battery is [x] degrees Celsius. The cycling consists of [A] charging stages. In the first stage, the battery was charged at a constant current of [x] C to [x]% state-of-charge (SOC). ... In the Ath stage, the battery was charged at a constant current of [x] C to [x]% SOC. The discharging consists of [B] stages. In the first stage, the battery was discharged at a constant current of [x] C to [x]% SOC. ... In the Bth stage, the battery was discharged at a constant current of [x] C to [x]% SOC. The cycling state-of-charge of this battery ranges from [x]% to [x].

Note: If there is only one charging/discharging stage, we will directly describe the single charging/discharging stage.

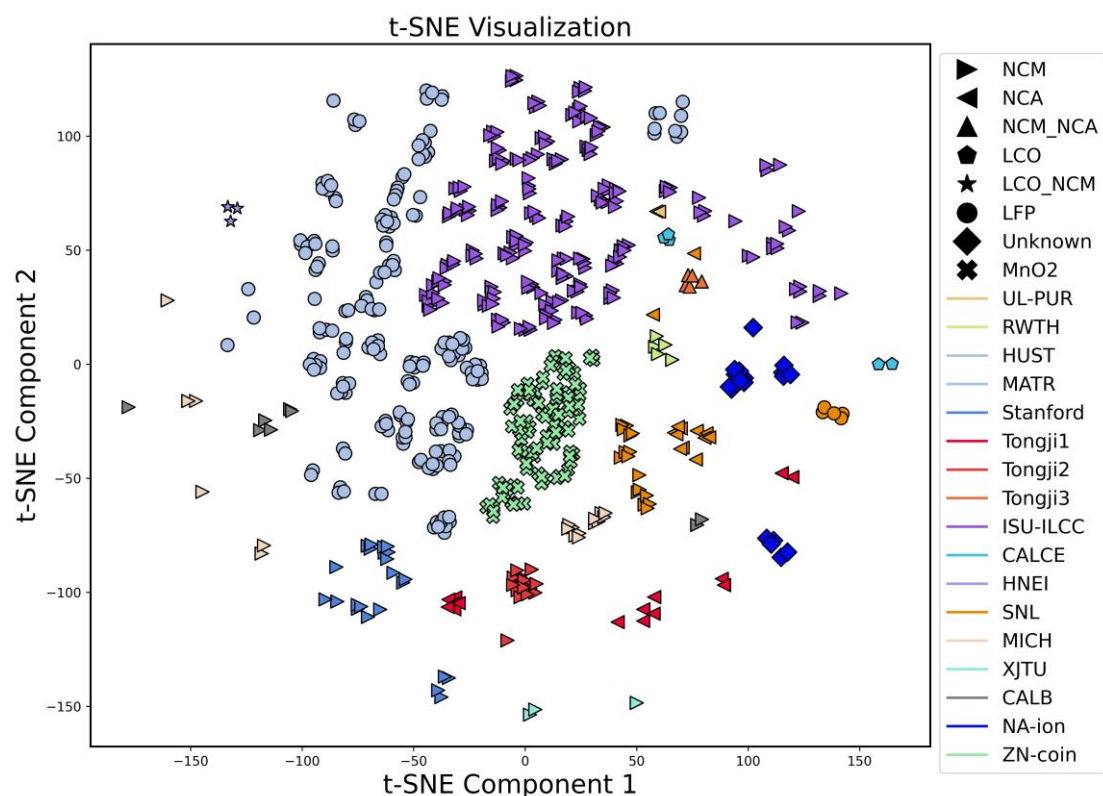
b

Task description: The target the number of cycles until the battery’s discharge capacity reaches 80% of its nominal capacity. The discharge capacity is calculated under the described operating condition. Please directly output the target of the battery based on the provided data.

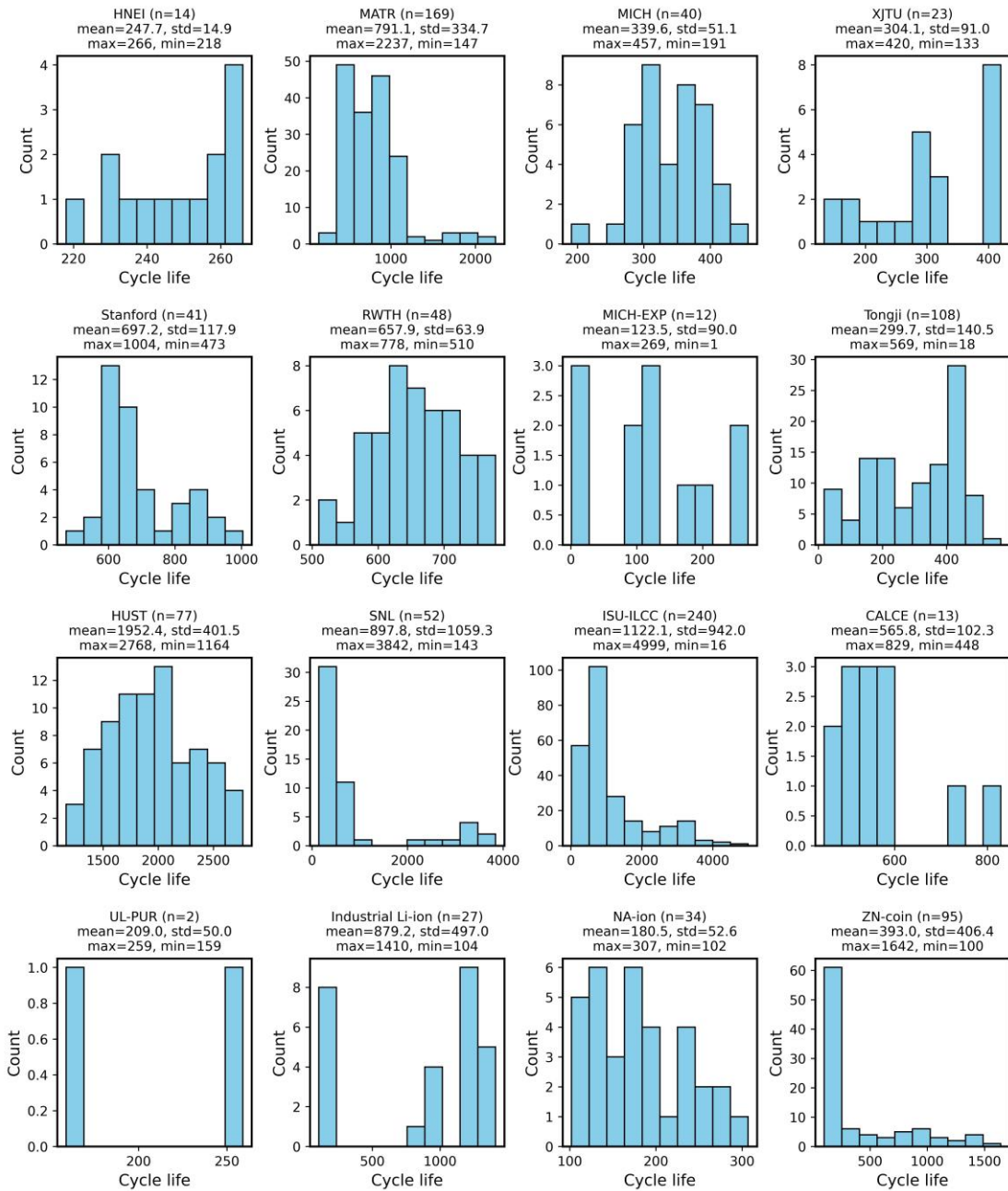
Battery specifications: The data comes from a lithium-ion battery in a format of 18650 cylindrical battery. Its positive electrode is a lithium iron phosphate (LiFePO₄). Its negative electrode is graphite. The electrolyte formula is unknown. The battery manufacturer is A123 system. The nominal capacity is 1.1 Ah.

Operating condition: The working history of this battery is just after formation. The working ambient temperature of this battery is 30 degrees Celsius. The cycling consists of four charging stages. In the first stage, the battery was charged at a constant current of 4.8 C to 20% state-of-charge (SOC). In the second stage, the battery was charged at a constant current of 5.2 C to 40% SOC. In the third stage, the battery was charged at a constant current of 5.2 C to 60% SOC. In the fourth stage, the battery was charged at a constant current of 4.16 C to 80% SOC until reaching 3.6 V. The battery was then discharged at a constant current of 4 C until reaching 2 V. The cycling state-of-charge of this battery ranges from 0% to 100%.

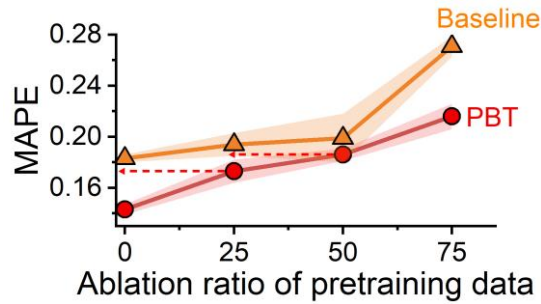
Supplementary Figure 2. The unified prompt template for the LLM-based ageing embedder and one example. a, the unified prompt template for the LLM-based ageing embedder. b, one example for one LiFePO₄/Graphite 18650 cylindrical battery.



Supplementary Figure 3. *t*-SNE visualization of prompt embeddings for the ageing conditions of training batteries generated by a large language model (LLM). Colors represent datasets, and shapes indicate cathode materials. In general, embeddings of ageing conditions within each dataset cluster in similar regions, indicating that the LLM recognizes the influence of battery specifications on ageing behavior. Batteries within the same dataset typically share identical specifications—except for the Tongji and SNL datasets, which include multiple chemistries and formats—leading to more dispersed clustering. Within each dataset, the embeddings remain distinguishable, suggesting that the LLM also captures variations arising from operating conditions and formation protocols. Moreover, embeddings of ageing conditions sharing the same cathode tend to cluster closely even across datasets. These results demonstrate the LLM’s prior understanding of battery ageing mechanisms and its capacity to generate physically meaningful vector representations.



Supplementary Figure 4. Battery life distributions across the 16 collected datasets. The title of each subpanel reports the dataset name and summary statistics. *Std* denotes the standard deviation, and n is the number of batteries that reached end of life. For the CALB dataset, most cells did not degrade to 80% of nominal capacity; therefore, the cycle number at 90% capacity is used as the life label following BatteryLife⁶.



Supplementary Figure 5. Model performance as a function of progressively reduced pretraining-data volume. Shaded regions represent standard deviations across three independent runs. The arrowed red lines denote the performance of PBT under varying data-ablation ratios, shown for comparison with the baseline models trained with more pretraining data. The baseline is the PBT without BatteryMoE.

Supplementary References

- 1 Zheng, H. *et al.* Learning from models beyond fine-tuning. *Nature Machine Intelligence* **7**, 6-17 (2025). <https://doi.org/10.1038/s42256-024-00961-0>
- 2 Loshchilov, I. & Hutter, F. in *7th International Conference on Learning Representations, ICLR 2019, May 6, 2019 - May 9, 2019*. (International Conference on Learning Representations, ICLR).
- 3 Ba, J. L. Layer normalization. *arXiv preprint arXiv:1607.06450* (2016).
- 4 Zhang, H. *et al.* Battery lifetime prediction across diverse ageing conditions with inter-cell deep learning. *Nature Machine Intelligence* (2025). <https://doi.org/10.1038/s42256-024-00972-x>
- 5 Dai, D. *et al.* in *62nd Annual Meeting of the Association for Computational Linguistics, ACL 2024, August 11, 2024 - August 16, 2024*. 1280-1297 (Association for Computational Linguistics (ACL)).
- 6 Tan, R. *et al.* in *Proceedings of the 31st ACM SIGKDD Conference on Knowledge Discovery and Data Mining V.2* 5789–5800 (Association for Computing Machinery, Toronto ON, Canada, 2025).